

Accretion indicators for the 37 brightest radio sources in the Subaru/*XMM-Newton* Deep Field

E. VARDOLAKI⁽¹⁾, S. RAWLINGS⁽¹⁾ and C. SIMPSON⁽²⁾

⁽¹⁾ *Astrophysics, Denys Wilkinson Building, Keble Road, Oxford, OX1 3RH, UK.*

⁽²⁾ *Astrophysics Research Institute, Liverpool John Moores University, Twelve Quays House, Egerton Wharf, Birkenhead CH41 1LD, UK.*

Summary. — We study the 37 brightest radio sources in the Subaru/*XMM-Newton* Deep Field (SXDF). Using mid-IR (Spitzer MIPS 24 μm) data we expect to trace nuclear accretion activity, even if it is obscured at optical wavelengths, unless the obscuring column is extreme. Our results suggest that above the ‘FRI/FRII’ radio luminosity break most of the radio sources are associated with objects that have excess mid-IR emission, only some of which are broad-line objects, although there is one clear low-accretion-rate FRI. The fraction of objects with mid-IR excess drops dramatically below the FRI/FRII break, although there exists at least one high-accretion-rate QSO. Investigation of mid-IR and blue excesses shows that they are correlated as predicted by a model in which a torus of dust absorbs $\sim 30\%$ of the light, and the dust above and below the torus scatters $\gtrsim 1\%$ of the light.

1. – Introduction and Data

Powerful radio sources are believed to have central super-massive black holes (SMBH) with uniformly high accretion rates at the highest radio luminosities and typically lower accretion rates at lower radio luminosities ([9]). Low-luminosity radio jets can, however, be associated with high-accretion-rate systems, and these so-called ‘radio quiet’ quasars appear to have similar FRI-like radio structures to low-accretion-rate counterparts of similar radio luminosity (e.g. [4]). At low redshift, the most massive ($\gtrsim 10^8 M_\odot$) SMBH typically have very low accretion rates with systematically higher average values at $z \gtrsim 2$, the so-called ‘quasar epoch’ ([14]). These observational results fit in with theoretical ideas that a ‘quasar mode’ of feedback is prevalent in the distant universe, and that a ‘radio mode’ feedback is dominant at low redshift (e.g. [2]).

The central region of an AGN is surrounded by a dusty torus which absorbs light and re-emits it in the infrared. Above and below the plane of the torus, dust scatters light yielding a blue excess. Such mechanisms make it difficult to observe objects viewed through the torus directly in the optical, UV and soft X-rays. The torus creates anisotropic obscuration of the central regions resulting in two different types of observed

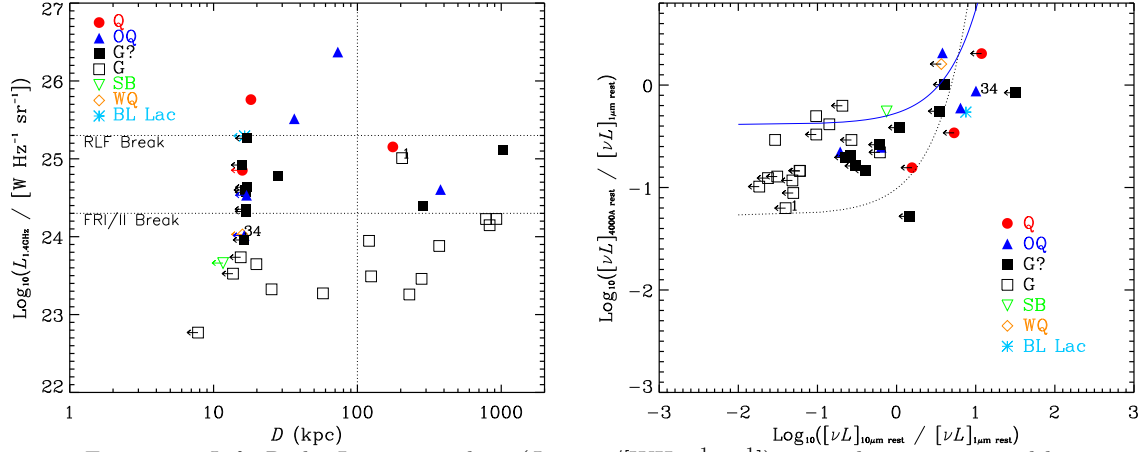


Fig. 1. – a *Left*: Radio Luminosity $\log_{10}(L_{1.4\text{GHz}} / [\text{W Hz}^{-1} \text{sr}^{-1}])$ versus largest projected linear size D : symbols indicate optical/IR classification; filled red circles for quasars 'Q'; filled blue triangles for obscured quasars 'OQ'; filled black squares for possible galaxies 'G?'; black squares for secure galaxies 'G'; green upside-down triangles for starbursts 'SB'; orange diamonds for weak quasars 'WQ'; and light blue stars for BL Lac 'BL'. The horizontal lines show the RLF and FRI/FRII breaks calculated from the values in [3] using a typical steep-spectrum spectral index of 0.8 and translated to our assumed cosmology. b *Right*: Blueness versus mid-IR excess. Symbols are the same as in the left figure. The black dotted line corresponds to the best-fit line in the log-linear plane where all objects, were treated as detections; the slope and intercept are 0.26 and -1.27 respectively, giving (see Eqn (2)) $k_1 = 0.05$ and $k_2 = 0.03$. The blue solid line corresponds to the best-fit line in log-linear plane where objects without detections at 24 μm were treated as limits; the slope and intercept are 0.10 and -0.41 respectively, giving $k_1 = 0.39$ and $k_2 = 0.09$. The Buckley-James method in the ASURV statistics package ([6]) was used in these calculations. 'SB' and 'BL' objects were excluded from the calculations since they have SEDs dominated by different physical processes to those assumed in the model described by Eqns (1) and (2). We adopt a radio spectral index $\alpha = 0.8$ ($S_\nu \propto \nu^{-\alpha}$), unless a spectral index could be calculated using 1.4 GHz data from [11] and 325 MHz data from [12] (see Vardoulaki *et al.* in prep.). We assume throughout a low-density, Λ -dominated Universe in which $H_0 = 70 \text{ km s}^{-1} \text{Mpc}^{-1}$, $\Omega_M = 0.3$ and $\Omega_\Lambda = 0.7$.

objects, type 1 that are viewed face-on and type 2 that are viewed edge-on. Here we use mid-IR observations to search for evidence of accretion in a manner which is far less dependent on orientation.

The sample studied here is the 37 brightest radio sources from the VLA survey of the Subaru/*XMM-Newton* Deep Field (SXDF; [11]) with flux densities greater than 2 mJy at 1.4 GHz. Optical, X-ray and radio observations of the SXDF were made within the 1.3 square degree Subaru/*XMM-Newton* Deep Field with Subaru, *XMM-Newton* and the VLA respectively. Thirteen of our objects are not as yet spectroscopically confirmed so we use photometric redshifts in these cases, calculated with the HYPERz code ([1]) and typically nine data points from B –band (440 nm) to 4.5 μm (Vardoulaki *et al.* in prep.).

2. – Discussion

We use optical/IR observations to classify a radio source as either Quasar 'Q', Obscured Quasar 'OQ', Galaxy? 'G?', Galaxy 'G', Starburst 'SB', Weak Quasar 'WQ' or BL Lac 'BL'. We deem that nuclear accretion is 'significant' in objects that obey

$\log_{10}(L_{24\mu\text{m}}/[\text{WHz}^{-1}\text{sr}^{-1}]) > 23.1$ (or $[\lambda L]_{24\mu\text{m}} > 10^{37.3}$ W). This value corresponds to $[\lambda L]_{24\mu\text{m}} \geq 10^{-1.8} L_{Edd}$, a typical lower limit for quasars ([7]), for a black hole mass $M_{\text{BH}} \geq 10^8 M_{\odot}$, a typical lower limit for radio sources ([8]); L_{Edd} is the Eddington luminosity. We then define the following categories:

- i) **Q**: Broad lines in the optical spectrum (3/37 cases). None of these are detected at 24 μm , although their limits are insufficient to rule out significant accretion.
- ii) **OQ**: Objects with a 24- μm detection (5/37 cases) and with sufficient L_{24} to represent significant accretion. This class may be incomplete in that some objects in the ‘G?’ class, as described next, have limits above this critical value.
- iii) **G?**: A galaxy that has a 24- μm limit consistent with it lying above the $\log_{10}(L_{24\mu\text{m}}/[\text{WHz}^{-1}\text{sr}^{-1}]) = 23.1$ line⁽¹⁾ (11/37 cases).
- iv) **G**: All other objects (15/37 cases) without significant accretion, unless they fall into three special categories defined by properties derived from spectroscopy, the SED and the optical structure: **SB**: evidence from the SED of a starburst component (1/37 cases); **WQ**: evidence from the SED of a quasar component but no 24 μm detection (1/37 cases); **BL**: featureless red continuum and a point source at K (1/37 cases).

Figure 1a shows the 1.4-GHz radio luminosity at $L_{1.4\text{GHz}}$ versus the projected linear size D with the symbols denoting the different optical/IR classes. We see that nearly all ‘Q’, ‘OQ’ and ‘G?’ objects of our sample lie above the ‘FRI/FRII’ luminosity break⁽²⁾, with the exception of the ‘OQ’ sxdf_0034 (the ‘G?’ object near sxdf_0034 lies very close to the boundary of significant accretion). In previous studies, the quasar fraction has been defined as the number of sources with quasar-like optical features (e.g. broad lines) and has a value of $\sim 0.1 \rightarrow 0.4$ over this range of $L_{1.4\text{GHz}}$ (e.g. [13]). We introduce the ‘quasar-mode fraction’ f_{QM} to describe the fraction of objects with high accretion rates to the total number of objects. Above the FRI/FRII break $f_{\text{QM}} \sim 0.5 - 0.9$ (the lower value assumes the 24 μm limits are much higher than the true 24 μm values, whereas the higher value assumes the true values lie just below the limits). The one clear exception in this regime is sxdf_0001, which has no evidence of a QSO and a clear Twin-Jet (FRI) radio structure.

The quasar-mode fraction drops dramatically below the FRI/FRII break⁽³⁾, and whether or not one excludes some of the compact ($D < 100$ kpc) sources as potentially part of a separate (beamed) population, then $f_{\text{QM}} \lesssim 0.1$ because nearly all objects are galaxies ‘G’. The counter example here are sxdf_0034, the only ‘OQ’ below the FRI/FRII break, and potentially an optically-obscured example of unobscured FRI QSOs already studied in this radio luminosity regime (e.g. [4]).

Inspection of the SEDs (Vardoulaki *et al.* in prep) shows that some of our objects have an excess at 24 μm above that expected from extrapolation of the stellar populations. This is quantified via a measure of the mid-IR excess, $\log_{10}([\nu L]_{10\mu\text{mrest}}/[\nu L]_{1\mu\text{mrest}})$. A comparison of mid-IR excess and blueness is presented in Fig. 1b where a positive

⁽¹⁾ Because of the 24 μm flux density limit, these objects are at high redshift, and hence, because of the 1.4-GHz flux density limit, a high- $L_{1.4\text{GHz}}$ sub-set of the objects lacking Spitzer 24 μm detections.

⁽²⁾ Although the FRI/FRII classification scheme is on the basis of radio structure, there is a sharp change in radio structure at a characteristic radio luminosity [3].

⁽³⁾ We note that objects in our sample above the FRI/FRII break have median redshift $z_{\text{med}} \sim 1.6$, whereas those below have $z_{\text{med}} \sim 0.65$, so evolutionary effects may also be important.

correlation is obvious. The generalised Spearman correlation calculated using survival analysis statistical package ASURV ([6]) is 0.657 with a 99% probability for a correlation.

Consider a simple model in which blueness is connected to mid-IR excess through the following equations⁽⁴⁾:

$$(1) \quad [\nu L]_{4000\text{Årest}} = k_1 \times [\nu L]_{1\mu\text{mrest}} + k_2 \times [\nu L]_{10\mu\text{mrest}} \Rightarrow$$

$$(2) \quad \log_{10} \left(\frac{[\nu L]_{4000\text{Årest}}}{[\nu L]_{1\mu\text{mrest}}} \right) = \log_{10}(e) \times \frac{k_2}{k_1} \times \left(\frac{[\nu L]_{10\mu\text{mrest}}}{[\nu L]_{1\mu\text{mrest}}} \right) + \log_{10}(k_1),$$

where k_1 encodes the contribution of the stellar population of a passively evolving galaxy formed at high redshift ($z > 5$), and k_2 the mid-IR-excess parameter that we are looking to calculate for this sample of radio sources. This model assumes that light from the nucleus with intrinsic optical luminosity L_{opt} is i) absorbed by dust and re-emitted in the mid-IR generating luminosity $[\nu L]_{10\mu\text{mrest}}$ and ii) scattered, generating luminosity $[\nu L]_{4000\text{Årest}}$. Fig. 1b shows best-fit lines for two scenarios: 1) all objects were treated as detections (black dotted line), and 2) objects are treated as upper limits according to their 24 μm detection (blue solid line), where in both cases ‘SB’ and ‘BL’ objects were excluded (Fig. 1b). Averaging these results we deduce $k_1 \sim 0.2$ and $k_2 \sim 0.05$, which agrees well with independent evidence. The value deduced for k_1 is in line with the expectations of template spectra of galaxies which formed their stars at high redshift. Optical polarisation studies (e.g. [5]) tell us that $[\nu L]_{4000\text{Årest}} \gtrsim 0.01 [\nu L]_{\text{opt}}$, which is consistent with our value of k_2 given that QSO SED studies suggest $[\nu L]_{10\mu\text{mrest}} \sim 0.3 [\nu L]_{\text{opt}}$ ([10]). We conclude that whenever nuclear accretion is significant in our sample of radio sources, dust in the torus absorbs 30% of the photons and dust above and below the torus scatters $\gtrsim 1\%$ of the photons.

* * *

REFERENCES

- [1] Bolzonella, M., *et al.*, 2000, A&A, 363, 476
- [2] Croton, D. J., *et al.*, 2006, MNRAS, 365, 11
- [3] Fanaroff, B. L., Riley, J. M., 1974, MNRAS, 167, 31
- [4] Heywood, I., *et al.*, 2007, astro-ph, arXiv0708.1145
- [5] Kishimoto, M., *et al.*, 2001, ApJ, 547, 667
- [6] Lavalley, M., *et al.*, 1992, ASPC, 25, 245
- [7] McLure, R. J., Dunlop J. S., 2004, MNRAS, 352, 1390
- [8] McLure, R. J., *et al.*, 2004, MNRAS, 351, 347
- [9] Rawlings, S. & Saunders, R., 1991, Nature, 349, 138
- [10] Rowan-Robinson, M., 1995, MNRAS, 272, 737
- [11] Simpson, C., *et al.*, 2006, MNRAS, 372, 741
- [12] Tasse, C., *et al.*, 2006, A&A, 456, 791
- [13] Willott, C. J., *et al.*, 2000, MNRAS, 316, 449
- [14] Yu, Q., Tremaine, S., 2002, MNRAS, 335, 965

⁽⁴⁾ Equation (2) relies on the $\ln(1 + x) \approx x$ approximation which is only accurate around and below the knees of the functions plotted in Fig. 1b.